ISSN: 0975-8585

Research Journal of Pharmaceutical, Biological and Chemical Sciences

The Influence of Aluminum on the Texture, Microstructure, Physical, Mechanical and Tribological Properties of $Ti_{1-x}Al_xN$ Thin Films.

A L Kameneva*.

Department of Innovative Engineering Technology, Perm National Research Polytechnic University / 614990, Perm, Komsomol'skiy pr. 29, Russia.

ABSTRACT

The temperature conditions for different formation stages of nanostructured and polycrystal $Ti_{1-x}Al_xN$ thin films have been identified for the first time, using cathodic arc evaporation. A three-axis structural zone model has been developed to identify structural zones of $Ti_{1-x}Al_xN$ thin films. This model, combined with chemical analysis, has been used to establish a pattern for $0 \le x \le 0.4$ in $Ti_{1-x}Al_xN$thin films with reference to the formation process and temperature conditions. Nanostructured $Ti_{0,6}Al_{0,4}N$ films formed at the maximum film heating rate and at the optimum gas mixture pressure have the highest aluminum content $C_{Al}=x$= 28.7 at.% and the film composition approaches the stoichiometric one. If the C_{Al} is higher than 26.5 at.% and the $C_{Al}/C_{Ti}=x/1-x$ is higher than 0.6, the size of the coherent scattering region (*CSR*) declines sharply to 10 nm. The degree of texturization of the $Ti_{1-x}Al_xN$ thin films steadily increases with the growth of the C_{Al} and C_{Al}/C_{Ti}. An improvement in physical and mechanical properties of $Ti_{1-x}Al_xN$ thin films can be achieved by bringing the C_{Al} to ≥ 26.5 at.%, by bringing the C_{Al}/C_{Ti} to ≥ 0.6, by reducing the *CSR* size to 10 nm, by ordering the microstructure, and by increasing the degree of texturization of $Ti_{1-x}Al_xN$ thin films to 0.8. The $Ti_{1-x}Al_xN$ thin films also exhibit excellent sliding wear resistance and a low friction coefficient due to maximum full free energy of 71.3 eV and Al_2O_3 layer which diminishes O_2 diffusion into $Ti_{1-x}Al_xN$ thin film and preserves its microhardness at high temperatures. If the C_{Al} and C_{Al}/C_{Ti} conditions are not met, the influence of $Ti_{1-x}Al_xN$ films on the properties is significant.

Keywords - $Ti_{1-x}Al_xN$ thin film; PVD; elemental composition; physical and mechanical properties, tribological properties

Corresponding author

ISSN: 0975-8585

INTRODUCTION

Preservation of physical, mechanical, thermal and tribological properties of $Ti_{1-x}Al_xN$ thin films (In that context, *C(Al)=x*- aluminum content, *C(Ti)=1-x*- titanum content, and *C(Al)/C(Ti)=(x/(1-x)* –aluminum-to-titanum content ratio) and substrate at rising temperature in the friction area can be assured by developing a highly adhesive Al_2O_3 surface layer which preserves microhardness at high temperatures due to diminished O_2 diffusion into $Ti_{1-x}Al_xN$ thin films, preventing their oxidation [1,2].

However, the above listed properties of $Ti_{1-x}Al_xN$ thin films with single-phase NaCl structure deteriorate significantly if the *C(Al)* goes up to x≥0.7. The wurtzite AlN structure created by phase transition from the cubic AlN structure results in incompatibility with the cubic solid solution. It also changes the electronic structure and bonding in the $Ti_{1-x}Al_xN$ thin film and causes its cohesive failure [3-5]. Numerous studies [6-10] have confirmed the influence which *C(Al)*, the deposition method and process conditions exert on the final properties of $Ti_{1-x}Al_xN$ thin films.

However, the influence patterns of *C(Al)* and *C(Al)/C(Ti)* with respect to the texture, the microstructure, physical, mechanical and tribological properties of $Ti_{1-x}Al_xN$ thin films have not been studied to a sufficient extent.

The objective of this paper is to study the influence of the *C(Al)* and *C(Al)/C(Ti)* on the texture, microstructure, physical and mechanical properties, and tribological properties, such as wear and friction resistance, of $Ti_{1-x}Al_xN$ thin films.

EXPERIMENTAL

Specimen preparation

The surface of all test samples – plates of VK8 hard alloy (substrate) – was subjected to ionic cleaning using a single arc evaporator with a Ti cathode. To obtain $Ti_{1-x}Al_xN$ thin films of various ultimate composition, the initial $Ti_{1-x}Al_xN$ thin film temperature (T_f) and heating rate ($V_{f.heat}$) were increased during deposition. The substrate temperature (T_{sub}), the heating rate ($V_{sub.heat}$), heating distribution and, as a consequence, T_f were increased without changing the time of ionic cleaning by raising the high voltage rates or by long-duration substrate pre-treatment at low temperature in glow discharge, or by increasing the length of ionic cleaning with gradual increase of high voltage. The $V_{f.heat}$ of $Ti_{1-x}Al_xN$ thin films during their deposition was increased by raising the technological parameters: gas mixture pressure (*P*) and bias voltage supplied to the substrate during the deposition process. Any changes in temperature were also assessed with respect to T_{sub}/T_{fm} (T_{fm} – thin film melting temperature) and $V_{f.heat}$. The surface temperature of the fixed substrate was taken after ionic cleaning and deposition of the sublayer TiN and $Ti_{1-x}Al_xN$thin films, using a Termix infrared noncontact pyrometer.

To identify the technological and temperature parameters at which the nanostructured and polycrystal $Ti_{1-x}Al_xN$ thin films were formed, their structure evolution was assessed in the ranges of low temperature (0.194 to 0.230)·T_{fm} and low pressure of the Ar and N_2 gas mixture (0.5 to 1.0 Pa), where formation of the microdrop phase is impossible.

Measurement techniques

Surface morphology and fractography of the fractures study

A surface morphology study and fractography of the fractures of the $Ti_{1-x}Al_xN$ thin films was carried out with the use of a scanning electron microscope BS 300 with an attachment EDAX Genesis 200 and field emission electron microscope Ultra 55 with EDX attachments.

Local chemical analysis

Local chemical analysis of selected areas on $Ti_{1-x}Al_xN$ thin films was conducted using field emission electron microscope Ultra 55 with EDX attachments, scanning electron microscopes BS 300 with an attachment EDAX Genesis 2000 and Leo 1430 VP with an INCA Energy-300 energy dispersive spectrometer. Quantitative electron microprobe analysis was conducted using a MAR-3 type X-ray microanalyzer at 20 kV accelerating voltage, 20 nA measuring current and 5 µm probe size.

X-ray investigation

Diffractograms of $Ti_{1-x}Al_xN$ thin film areas were taken using a Shimadzu XRD-6000 X-ray diffractometer in Cu-Kα radiation at 30 kV voltage and 20 µA current. The angular spacing of the pictures taken was 2θ = 30 to 130^0, the exposure was at the 4 s point.

The crystal lattice parameter was calculated according to Vegard's law or the rule of additivity using the methodology described in publications [7] based on identifying the crystal lattice parameter of $Ti_{1-x}Al_xN$ solid solution followed by finding the quantity of the replacing component, assuming that its relation to the solid solution composition a(x) can be expressed as $a(x) = x \cdot a_{AlN} + (1 - x) \cdot a_{TiN}$, whence $x = [a_{TiN} - a(x)] / (a_{TiN} - a_{AlN})$. The crystal lattice parameter of the $Ti_{1-x}Al_xN$ solid solution was determined from the peak whose angular position corresponded to the double Bragg angle 2θ = 72 to $75^0$and peak positions (311) for TiN and AlN. Vegard's law is quite often not very accurately followed and can show deviations (convex and concave curves); however, the reading of C(Al) allows a 90% confidential probability.

The coherent scattering region size was calculated using the methodology reported in publication [8]. The degree of texturization (grain disorientation relative to the texture axis) of $Ti_{1-x}Al_xN$ thin films was calculated using $T = maxI_{107} / I_{\Sigma}$. The full free energy of $Ti_{1-x}Al_xN$ thin films surface (E_f) was assessed using the method described in thesis [5].

Mechanical test

The physical and mechanical properties of the $Ti_{1-x}Al_xN$ thin films: microhardness (H), Young's modulus (E), resistance to elastic failure strain (H/E), resistance to plastic strain (H^3/E^2) and elastic recovery (We) were measured according to the standard DINENISO 14577-1 method of nanoindentation, using FISCHERSCOPE H100C to measure thin films, as well as mathematical treatment of the obtained experimental curve series for load/unload test samples [9].

Wear test

Finger-on-disc wear tests of $Ti_{1-x}Al_xN$ thin films on flat substrates were undertaken against VK8 hard alloy at $25\ ^0$C in coolant-cutting fluid (Fig. 1,a). The number of fingers (counter body) was 3 (Fig. 1,b), the radius of the finger sphere was R = 6.5 ± 0.25 mm. The axial loading on three fingers was F_a = 175 H, the linear sliding velocity of the finger was V = 0.68 m/s. The rubbing path of the fingers was $L_т$ = 1500 m, the test duration was t = 740 s. The radius of thin film worn surfaces was R = 7 mm. Profilograms of the worn $Ti_{1-x}Al_xN$ thin film and finger surfaces were obtained and processed using a MarForm MMQ 400 high-precision out-of-round gage, running the MarShellMarWin software.

The tribological properties of $Ti_{1-x}Al_xN$ films: *friction resistance* – friction factor (*f*), frictional torque (M_f[1]), and counterbody wear resistance I_c^V were determined by the equations [10,11] (1), *wear resistance* – wear resistance in volume I_f^V and wear resistance in mass I_f^m were determined by the equations [7] (2).

$$f = \frac{M_f}{F_a \cdot r} = \frac{F_D \cdot l_D}{F_a \cdot r},\ I_c^V = \Delta V_c/(F_a \cdot L_m),\ \Delta V_c = \pi * h^2(R - 1/3h),\ h = R - (R^2 - d^2/4)^{1/2} \quad (1)$$

[1] For the moment, and the friction factor to the average values from those obtained for 3 seconds after passing the fingers sliding distance of 10 m.

ISSN: 0975-8585

$$I_f^V = \Delta V_f/(F_a \cdot L_m),\ V_f = d_f/t,\ \Delta V_f = \pi \cdot D \cdot \bar{S},\ I_f^m = \Delta m/(F_a \cdot L_m),\ \Delta m = m_1 - m_2, \quad (2)$$

where F_D is the force influencing the strain-gauge transducer (N); l_D is the distance from the rotation axis of holder **5** to the force strain-gauge transducer **8** (mm); m_1 is the weight of the sample with $Ti_{1-x}Al_xN$ thin film before, and m_2 after, testing (weighing error ± 0.15 mg) (mg). For the $Ti_{1-x}Al_xN$ thin film, V_f is the wear rate (mm^3), d_f is the diameter of the wear scar (mm), D is the diameter of the wear crater (mm) and $\bar{S}$ is the average area of the wear crater cross section (mm^2). For the counter body, ΔV_c is the decline in volume (mm^3), h is the height of the worn segment in mm and d_c is the diameter of the wear scar (mm).

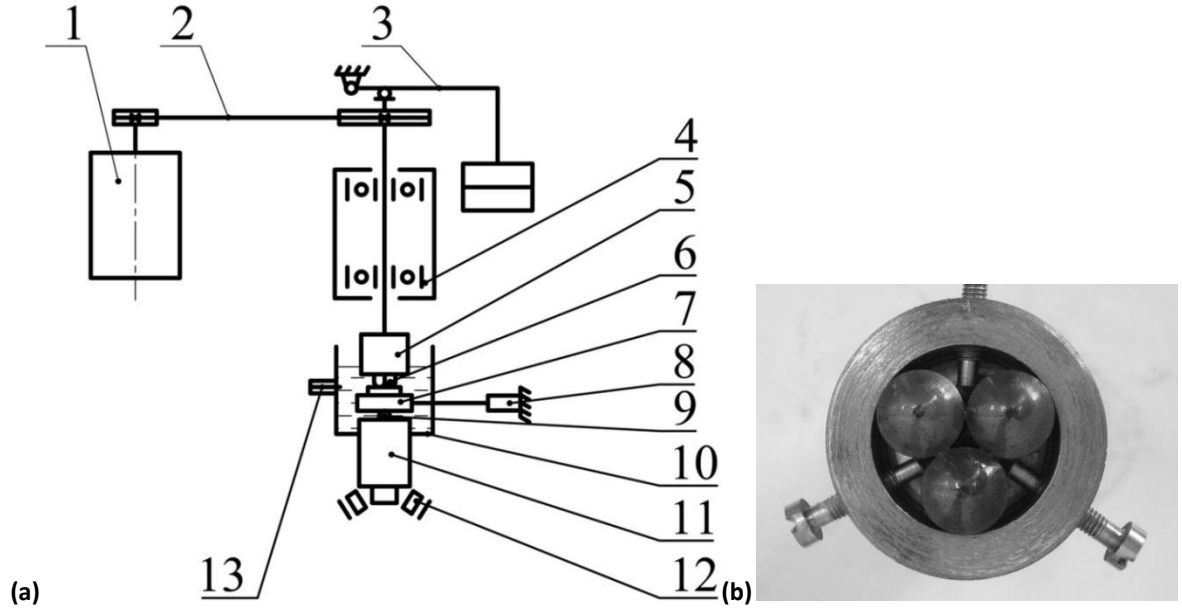

Fig. 1: (a) Friction machine for finger-on-disc wear tests of the $Ti_{1-x}Al_xN$ thin films:
1 – motor set; 2 – belt transmission; 3 – lever device with fractional weights; 4 – bearing support; 5 – holder; 6 – finger - counter body; 7 – disk with the sample (test sample with the $Ti_{1-x}Al_xN$ thin film applied on it) and a lever; 8 – strain gage force transducer; 9 – ball; 10 – a glass with coolant-cutting fluid; 11 – stationary base; 12 – bearing part. (b) Finger surfaces

RESULTS AND DISCUSSION

Influence of deposition conditions on the microstructure of $Ti_{1-x}Al_xN$ thin films and their Al content

Based on the results of the technology experiment, a surface morphology study and fractography of the fractures of the $Ti_{1-x}Al_xN$ thin films has been undertaken, for the first time, the temperature conditions have been identified for different formation stages of nanostructured and polycrystal $Ti_{1-x}Al_xN$ thin films, using cathodic arc evaporation. To build the three-axis structural zone model of $Ti_{1-x}Al_xN$ thin films, we developed schematic images for resultant structural formations and conventional signs for thin film formation stages:

1 –globules form and merge (Fig. 2,a);
2 – {100} edges develop on globules (Fig. 2,b);
3 – polycrystal component seeds of $Ti_{1-x}Al_xN$ thin film start to generate and intergrow (Fig. 2,c);
4 – geometric selection (Fig. 2,d);
5 –initial axial <100> structure forms (Fig. 2,e);
6 – texturing the crystallites into the plateletlike formations (Fig. 2,f);
5* – disordering between texture grains is reduced, nanostructuring of the crystallites and a solid nanostructured $Ti_{1-x}Al_xN$ thin film with a homogeneous (even) structure develops in the formation direction (Fig. 2,g).

ISSN: 0975-8585

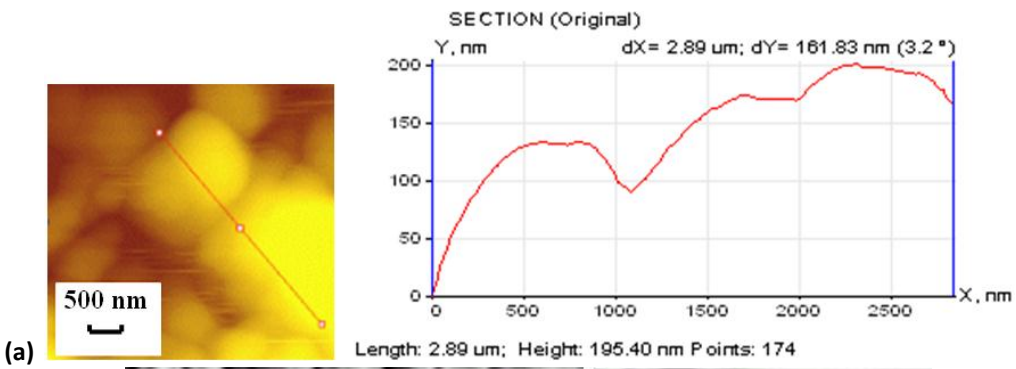

(a)

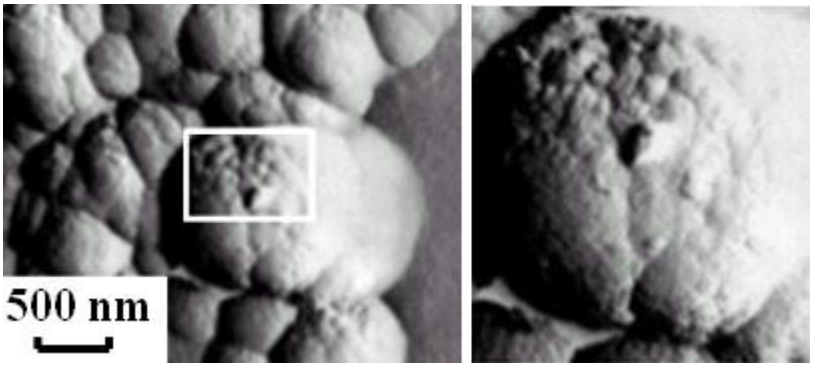

(b)

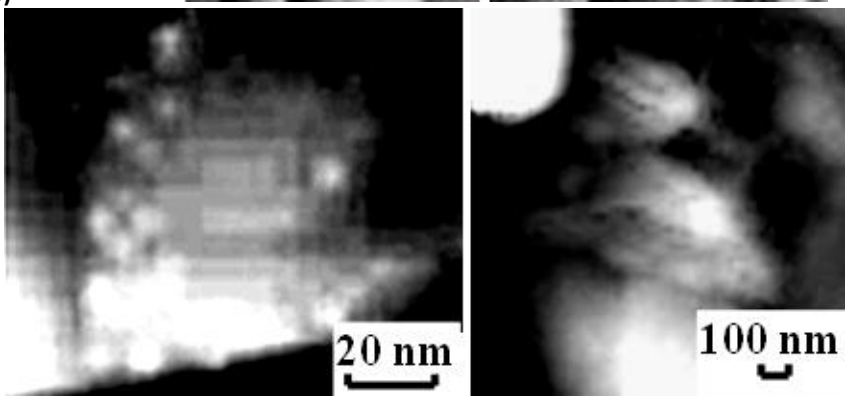

(c)

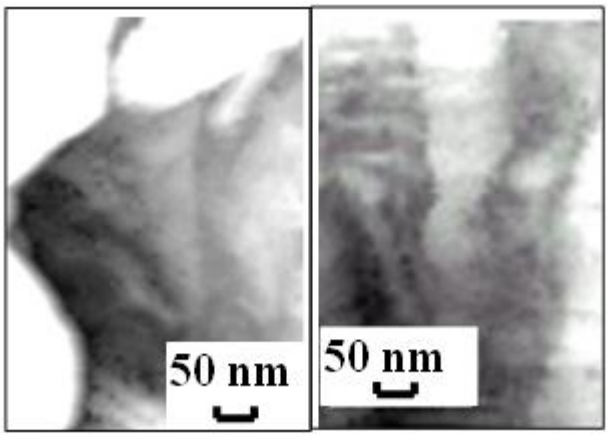

(d)

ISSN: 0975-8585

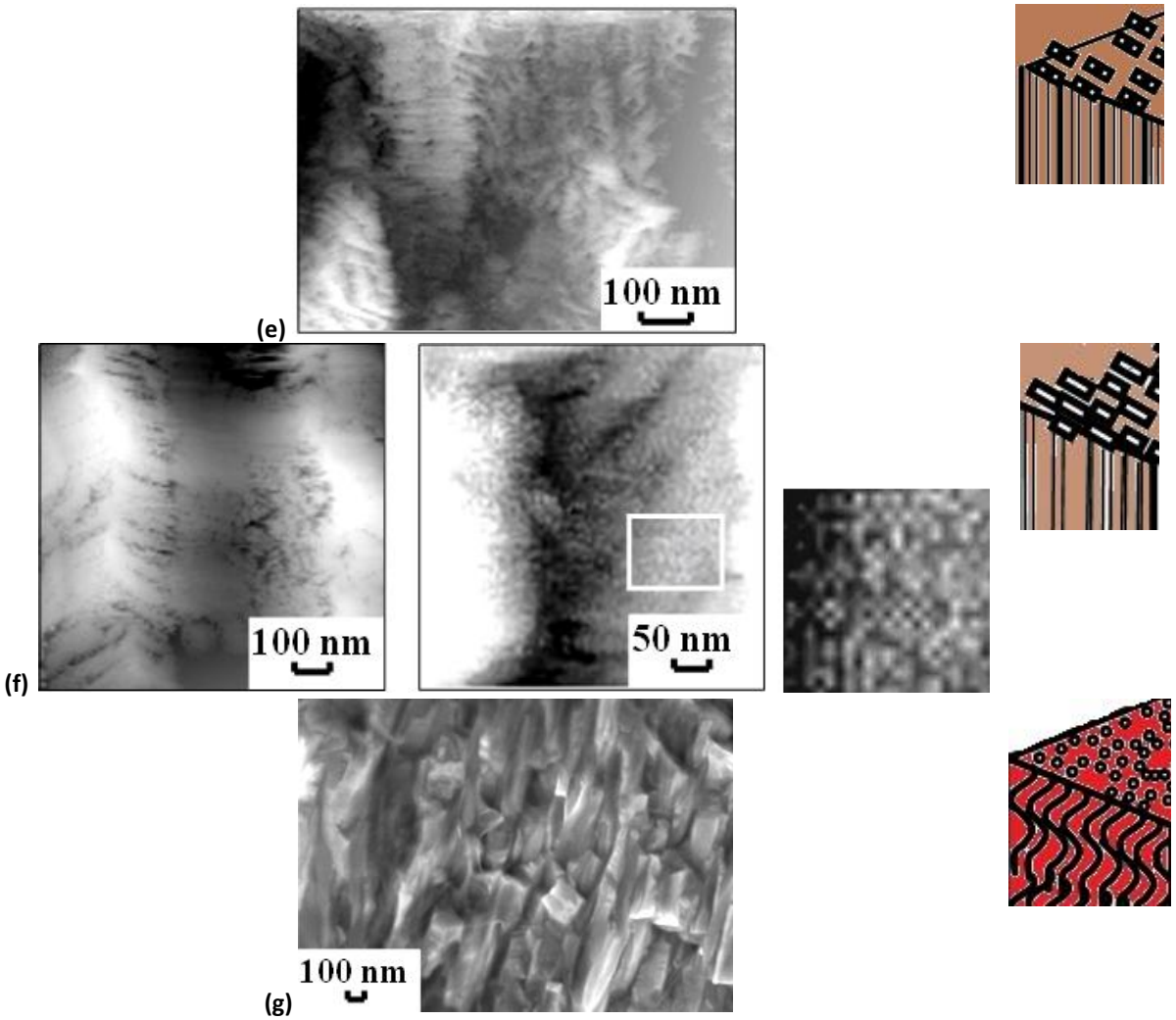

Fig. 2: The stages of thin $Ti_{1-x}Al_xN$ film formation

Based on the three-axis structural zone model (Fig. 3), structural changes in $Ti_{1-x}Al_xN$ thin films were identified depending on the technological and temperature parameters of the deposition process of cathodic arc evaporation, as well as the ability of nanostructured $Ti_{1-x}Al_xN$ thin films to form in a low-temperature area under the optimum structuring conditions. It is revealed that, under rapid substrate heating and minimal temperature of the deposition process, the rate of formation stages of the film decreases and the structural formation of the thin film is limited only by the globular stage.

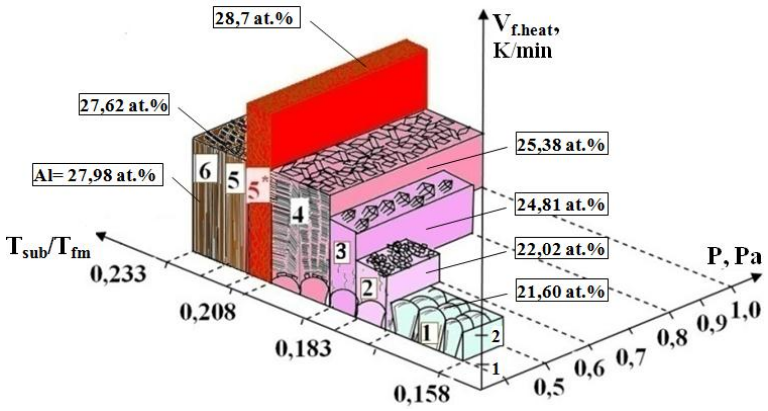

Fig. 3: Three-axis structural zone model of $Ti_{1-x}Al_xN$ thin films: T_{sub}/T_{fm}, $V_{f.heat}$ and gas mixture pressure. Numbers 1 to 6 in the model designate the stages of thin film formation [12-13]

ISSN: 0975-8585

Chemical analysis of $Ti_{1-x}Al_xN$ thin films at each stage of formation allowed us to conclude that ordering of the microstructure and increasing the degree of texturization was accompanied by an increase of the *C(Al)* in thin films. Nanostructured $Ti_{0,6}Al_{0,4}N$ thin films formed at the minimum substrate heating rate $V_{sub.heat}$ of 25 K/min, at the optimum initial thin film temperature of 670 K, at the maximum film heating rate $V_{f.heat}$ of 6 K/min, and at the optimum gas mixture pressure P of 1.0 Pa have the highest aluminum content *C(Al)* = 28.7 at.% and their composition approaches the stoichiometric one.

Influence of Al content on the $Ti_{1-x}Al_xN$ thin film texture

With the increase of gas mixture pressure, the quantity of triple $Ti_{1-x}Al_xN$ nitride, *C(Al)* and *C(Al)/C(Ti)* grows, in as much as the speed of plasma chemical reactions grows and so does the quantity of N_2 in the gas mixture which enters into a nitride formation reaction. With the growth of *C(Al)* in $Ti_{1-x}Al_xN$ thin film, the crystal lattice parameter value becomes reduced (this is evidenced in publications [1,8,14]). This is caused by smaller-sized Al atoms replacing Ti atoms in the TiN lattice, even though the coordination number of Ti and N_2 atoms in TiN is 6, while the coordination number of Al and N_2 atoms in AlN is 4. The reduction of $V_{sub.heat}$ during heat treatment of the substrate before $Ti_{1-x}Al_xN$thin film deposition also causes an increase of the *C(Al)* and a reduction in crystal lattice parameter value, due to a higher mobility of adsorbed atoms.

The *C(Al)* and the *C(Al)/C(Ti)* exert a significant influence on the size of the coherent scattering region and the degree of $Ti_{1-x}Al_xN$ thin film texturization. The increase of the *C(Al)* and *C(Al)/C(Ti)* to 26.5 at.% and 0.6 at.% respectively helps to reduce the size of the coherent scattering region and enhance the degree of $Ti_{1-x}Al_xN$ thin films texturization. If C_{Al}> 26.5 at. % and C_{Al}/C_{Ti}> 0.6, the size of the coherent scattering region declines sharply to 10 nm and the degree of $Ti_{1-x}Al_xN$ thin film texturization increases to 0.8 (Fig. 4).

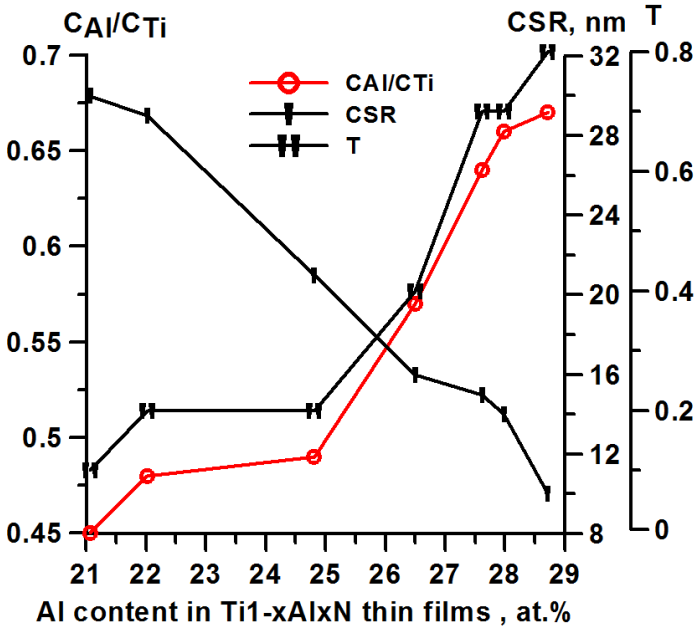

Fig. 4: Dependence of the size of the coherent scattering region and the degree of $Ti_{1-x}Al_xN$thin film texturization on *C(Al)* and *C(Al)/C(Ti)* in $Ti_{1-x}Al_xN$ thin films

Influence of Al content on the physical and mechanical properties of $Ti_{1-x}Al_xN$ thin films

Bringing the $Ti_{1-x}Al_xN$ thin film formation process into a higher temperature range, increasing the *C(Al)* to 26.5 at.%, ordering the thin film microstructure, reducing the size of the coherent scattering region and assuring a higher degree of $Ti_{1-x}Al_xN$ thin film texturization result in improved physical and mechanical properties of the thin films (Table, Fig. 5, a).

ISSN: 0975-8585

Table 1: Changes in tribological properties, physical and mechanical properties of $Ti_{1-x}Al_xN$ thin films depending on the *C(Al)* and *C(Al)/C(Ti)*

Al, at.%	C_{Al}/C_{Ti}	*H*, GPa	*E*, GPa	*H/E*	H^3/E^2, GPa	W_e, %	I_f^m, $\cdot 10^{-5}$ mg/N·m	I_f^V, $\cdot 10^{-4}$ mm^3/N·m	I_c^V, $\cdot 10^{-8}$ mm^3/N·m	f
21,06	0.45	26	197	0.10	0.36	53	12.25	7.53	10.15	0.18
22,02	0.48	27	274	0.10	0.42	55	11.75	6.96	9.56	0.17
24,81	0.52	28	280	0.10	0.43	58	9.24	6.59	7.26	0.15
26.50	0.61	32	303	0.10	0.70	66	7.80	3.50	3.77	0.13
27.62	0.64	33	329	0.10	0.79	68	1.06	0.38	0.78	0.11
27.98	0.66	34	334	0.10	0.94	69	0.12	0.26	0.43	0.09
28.70	0.67	36	358	0.11	1.31	76	0.03	0.05	0.18	0.08

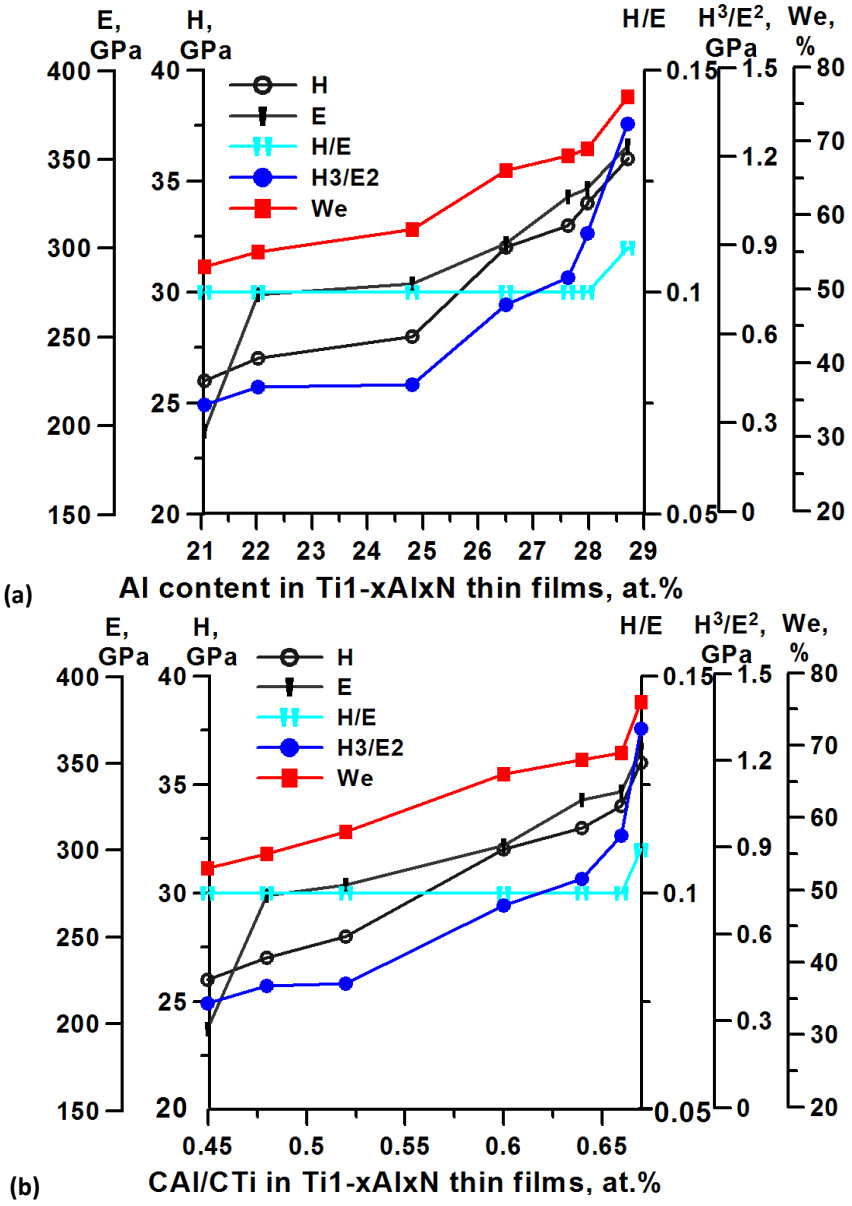

Fig. 5. The pattern of change in physical and mechanical properties of $Ti_{1-x}Al_xN$ thin films depending on their *C(Al)* (a) and *C(Al)/C(Ti) (b)*

ISSN: 0975-8585

The *C(Al)* value has only an insignificant impact on the $Ti_{1-x}Al_xN$ thin film resistance to *H/E* elastic failure strain, as the H and E values increase simultaneously with the growth in the *C(Al).*

The best collection of physical and mechanical properties, which is *H* = 36 GPa; *E* = 358 GPa; W_e = 76%; *H/E* = 0.10 and H^3/E^2 = 1.31 GPa, corresponds to nanostructured $Ti_{1-x}Al_xN$ thin film with the maximum *C(Al)* = 28.7 at.% and with the maximum *C(Al)/C(Ti)* = 0.67, formed under the optimum technological and temperature parameters.

The physical and mechanical properties of $Ti_{1-x}Al_xN$ thin films are more influenced by C_{Al}/C_{Ti} and by the extent to which the thin film composition matches the stoichiometric one (Fig. 5, b).

When the *C(Al)/C(Ti)* value in nanostructured $Ti_{1-x}Al_xN$ thin films increases, their elastic recovery improves and the thin films become more resistant to elastic failure strain and plastic deformation (Fig. 5, b). The efficiency of $Ti_{1-x}Al_xN$ thin films in terms of higher heat resistance and preservation of physical and mechanical properties of the substrate is due to formation of Al_2O_3 which preserves the properties both of thin film and substrate.

Influence of Al content on the tribological properties of $Ti_{1-x}Al_xN$ thin films

The durability and antifriction properties of $Ti_{1-x}Al_xN$ thin films are influenced by the *C(Al), C(Al)/C(Ti)*, the size of the coherent scattering region (*CSR*), surface deficiency, and full free energy of $Ti_{1-x}Al_xN$ thin film surface (E_f) (Fig. 6).

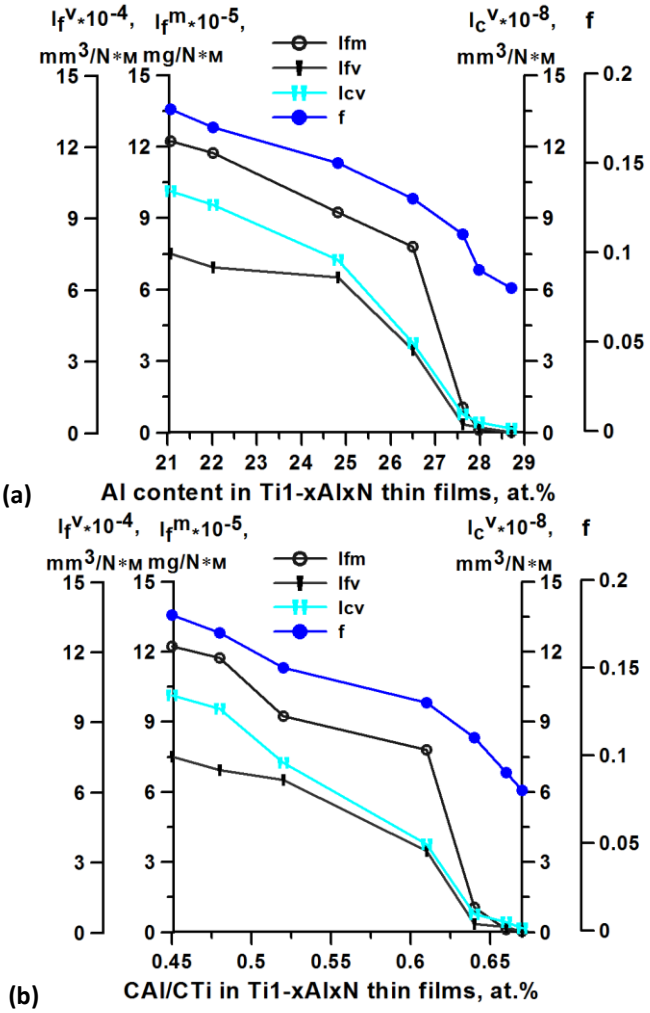

Fig. 6: The pattern of change in tribological properties of $Ti_{1-x}Al_xN$ thin films depending on the *C(Al) (a), C(Al)/C(Ti), E_f,* and *CSR* (b)

All tribological properties improve if the *C(Al)* value and *C(Al)/C(Ti)* value in the $Ti_{1-x}Al_xN$ thin films grows. Such an outcome of chemical analysis can be accounted for by the fact that the composition of $Ti_{1-x}Al_x$ N thin film is close to the stoichiometric one.

Analysis of the tribological properties: I_f^V, I_f^m, I_c^V and *f* shows that $Ti_{1-x}Al_xN$ thin films with $C_{Al} \geq$ 26.5 at.%, $C_{Al}/C_{Ti} \geq 0.6$, the smallest size of the coherent scattering region 10 nm, and the maximum full free energy of $Ti_{1-x}Al_xN$ thin film surface 71.3 eV have higher tribological properties (Fig. 6, Tab.). If the C_{Al} and C_{Al}/C_{Ti} conditions are not met, their influence on the tribological properties of $Ti_{1-x}Al_xN$ thin films is significant.

If the *C(Al)/C(Ti)* value in nanostructured $Ti_{1-x}Al_xN$ thin films increases to ≥ 0.60 and full free energy of the thin film surface goes up to 71.3 eV, the thin film and counterbody become more resistant to wear in volume and mass, and the friction factor goes down (Fig. 6, b). A higher wear resistance of $Ti_{1-x}Al_xN$ thin films results in a better preservation of both the thin film properties and counterbody properties.

CONCLUSIONS

A universal model of structural zones has been built and an opportunity has been identified to obtain nanostructured and polycrystal $Ti_{1-x}Al_xN$ thin films using cathodic arc evaporation at low values of substrate temperature and gas mixture pressure. Patterns of change have been traced for the microstructure, *C(Al)*, and *C(Al)/C(Ti)* associated with the technological and temperature parameters of the main process for $Ti_{1-x}Al_xN$ thin film deposition.

For the first time it has been ascertained that all tribological, physical and mechanical properties improve if the *C(Al)* value and *C(Al)/C(Ti)* value grows. Such an outcome of chemical analysis can be accounted for by the fact that the composition of $Ti_{1-x}Al_xN$ thin film is close to the stoichiometric one.

For the first time, the role of the *C(Al)* and *C(Al)/C(Ti)* has been determined, as well as that of the texture and microstucture of $Ti_{1-x}Al_xN$ thin films in developing their tribological, physical and mechanical properties.

The criteria for choosing a structure and composition of $Ti_{1-x}Al_xN$ thin films with a set of high tribological, physical and mechanical properties are: the size of the smallest coherent scattering region, high degree of $Ti_{1-x}Al_xN$ thin film texturization, maximum *C(Al)*, maximum *C(Al)/C(Ti)*, and maximum full free energy of the $Ti_{1-x}Al_xN$ thin film surface [15-18].

The resultant multi-factor relations of the *C(Al)* to the tribological, physical and mechanical properties confirm that the developed $Ti_{1-x}Al_xN$ thin film deposition processes allow us to obtain multifunctional thin films with a predetermined texture, composition and collection of tribological, physical and mechanical properties, to achieve a manifold increase in the resistance of process tools and friction pairs working with heavy-duty materials.

It is possible to manage the tribological, physical and mechanical properties of nanostructured $Ti_{1-x}Al_xN$ thin films by changing their *C(Al)* and *C(Al)/C(Ti)*.

Highlights

- Three-axis structural zone model of $Ti_{1-x}Al_xN$ thin films
- Interrelationships between the structure of $Ti_{1-x}Al_xN$ thin film and their properties
- Physical and mechanical properties of $Ti_{1-x}Al_xN$ thin films
- Tribological properties of $Ti_{1-x}Al_xN$ thin films
- $Ti_{1-x}Al_xN$ thin films with more than 26.5 at.% of Al content exhibit optimal properties

Abbreviations

C_{Al} - aluminum content,
C(Ti) - titanum content,
H – thin film microhardness,
E – thin film Young's modulus,

C_{Al}/C_{Ti} - aluminum to titanum content ratio,
T_f - thin film temperature,
T_{fm} – thin film melting temperature,
T_{sub} - substrate temperature,
$V_{f.heat}$ - thin film heating rate,
$V_{sub.heat}$ - substrate heating rate,
E_f - full free energy of thin film surface,
CSR - coherent scattering region,
T - maxI_{107} / I_{Σ} - degree of texturization,
H/E – thin film resistance to elastic failure strain,
H^3/E^2 – thin film resistance to plastic strain,
We - thin film elastic recovery,
I_f^V - thin film wear resistance in volume,
I_f^m - thin film wear resistance in mass,
f – thin film friction factor,
I_c^V - counterbody wear resistance in volume.

REFERENCES

[1] PalDey S, Deevi SC. J Mat Sci Eng. A 2003;342(1):58-79.
[2] Knotek O, Böhmer M, Leyendecker T, Jungblut F. J Mat Sci Eng A 1988;105–106(2):481-8.
[3] Hörling A, Hultman L, Odén M, Sjölén J, Karlsson L. J Surf Coat Tech 2005;191(2–3):384-392.
[4] Mayrhofer PH, Hörling A, Karlsson L, Sjölén J, Larsson T, Mitterer C, Hultman L. J Appl Phys Lett 2003;10:2049-2051.
[5] Höglund C. Growth and phase stability studies of epitaxial Sc-Al-N and Ti-Al-N thin films. Linköping: Linköpings University: 2010.
[6] Kameneva AL. J Design Comp Mater 2014;2:40-5.
[7] Holec D, Rachbauer R, Chen L, Wang L, Luef D, Mayrhofer PH. J Surf Coat Tech 2011;206(7):1698-1704.
[8] Gorelik VS, Friman AV. J Bull Lebedev Phys Inst 2011;38(4):105-10.
[9] Kameneva AL, Karmanov VV. J Alloys Comp 2013;546:20-7.
[10] Kameneva AL, Karavaev DM, Pepelyshev AV, Pimenova NV. J Technol Metals 2012;2:34-7.
[11] Zhou Z, Rainforth WM, Luo Q, Hovsepian PEh, Ojeda JJ, Romero-Gonzalez ME. Acta Materialia 2010;58(8):2912-5.
[12] Kameneva AL. Powder Metallurgy And Functional Coatings. 2011;4:41-8.
[13] Kameneva AL. J Russian J Non-Ferrous Metals 2013;54(6):541-7.
[14] Ikeda T, Satoh H. J Thin Solid Thin films 1991;195:99–110.
[15] Antsiferov VN, Kameneva AL. Patent 2433209; Russia.
[16] Antsiferov VN, Kameneva AL, Klochkov AY, Novikov RS. Patent 2361013; Russia.